Plasmon-enhanced LT-GaAs/AlAs heterostructure photoconductive antennas for sub-bandgap terahertz generation

Afshin Jooshesh, Faezeh Fesharaki, Vahid Bahrami-Yekta, Mahsa Mahtab, Thomas Tiedje, Thomas E. Darcie, and Reuven Gordon

September 2017

This article was originally published at:
https://doi.org/10.1364/OE.25.022140

Research Article Vol. 25, No. 18 | 4 Sep 2017 | OPTICS EXPRESS 22140

Optics EXPRESS

Plasmon-enhanced LT-GaAs/AlAs heterostructure photoconductive antennas for sub-bandgap terahertz generation

Afshin Jooshesh, Faezeh Fesharaki, Vahid Bahrami-Yekta, Mahsa Mahtab, Thomas Tiedje, Thomas E. Darcie, and Reuven Gordon*

Department of Electrical and Computer Engineering, University of Victoria, 3800 Finnerty Road, Victoria, British Colombia V8P 5C2, Canada

**rgordon@uvic.ca*

Abstract: Photocurrent generation in low-temperature-grown GaAs (LT-GaAs) has been significantly improved by growing a thin AlAs isolation layer between the LT-GaAs layer and semi-insulating (SI)-GaAs substrate. The AlAs layer allows greater arsenic incorporation into the LT-GaAs layer, prevents current diffusion into the GaAs substrate, and provides optical back-reflection that enhances below bandgap terahertz generation. Our plasmon-enhanced LT-GaAs/AlAs photoconductive antennas provide 4.5 THz bandwidth and 75 dB signal-to-noise ratio (SNR) under 50 mW of 1570 nm excitation, whereas the structure without the AlAs layer gives 3 THz bandwidth, 65 dB SNR for the same conditions.

OCIS codes: (250.5403) Plasmonics; (160.5140) Photoconductive materials; (040.2235) Far infrared or terahertz.

References and links

1. J. Orenstein and J. S. Dodge, "Terahertz time-domain spectroscopy of transient metallic and superconducting states," Phys. Rev. B **92**(13), 134507 (2015).
2. H. Y. Hwang, S. Fleischer, N. C. Brandt, B. G. Perkins, Jr., M. Liu, K. Fan, A. Sternbach, X. Zhang, R. D. Averitt, and K. A. Nelson, "A review of non-linear terahertz spectroscopy with ultrashort tabletop-laser pulses," J. Mod. Opt. **62**(18), 1447–1479 (2015).
3. A. Urbanowicz, V. Pačebutas, A. Geižutis, S. Stanionytė, and A. Krotkus, "Terahertz time-domain-spectroscopy system based on 1.55 μm fiber laser and photoconductive antennas from dilute bismides," AIP Adv. **6**(2), 025218 (2016).
4. N. Q. Vinh, M. S. Sherwin, S. J. Allen, D. K. George, A. J. Rahmani, and K. W. Plaxco, "High-precision gigahertz-to-terahertz spectroscopy of aqueous salt solutions as a probe of the femtosecond-to-picosecond dynamics of liquid water," J. Chem. Phys. **142**(16), 164502 (2015).
5. P. U. Jepsen, D. G. Cooke, and M. Koch, "Terahertz spectroscopy and imaging - Modern techniques and applications," Laser Photonics Rev. **5**(1), 124–166 (2011).
6. R. Faulks, S. Rihani, H. E. Beere, M. J. Evans, D. A. Ritchie, and M. Pepper, "Pulsed terahertz time domain spectroscopy of vertically structured photoconductive antennas," Appl. Phys. Lett. **96**(8), 081106 (2010).
7. P. Y. Han and X. C. Zhang, "Free-space coherent broadband terahertz time-domain spectroscopy," Meas. Sci. Technol. **12**(11), 1747–1756 (2001).
8. D. Grischkowsky, S. Keiding, M. Exter, and C. Fattinger, "Far-infrared time-domain spectroscopy with terahertz beams of dielectrics and semiconductors," J. Opt. Soc. Am. B **7**(10), 2006 (1990).
9. S. F. Busch, G. E. Town, M. Scheller, and M. Koch, "Focus free terahertz reflection imaging and tomography with bessel beams," J. Infrared Millim. Terahertz Waves **36**(3), 318–326 (2015).
10. B. B. Hu and M. C. Nuss, "Imaging with terahertz waves," Opt. Lett. **20**(16), 1716–1718 (1995).
11. C. Jansen, S. Wietzke, O. Peters, M. Scheller, N. Vieweg, M. Salhi, N. Krumbholz, C. Jordens, T. Hochrein, and M. Koch, "Terahertz imaging: Applications and perspectives," Appl. Opt. **49**(19), E48–E57 (2010).
12. I. Kasalynas, R. Venckevicius, and G. Valusis, "Continuous wave spectroscopic terahertz imaging with InGaAs Bow-Tie diodes at room temperature," IEEE Sens. J. **13**(1), 50–54 (2013).
13. K. Serita, S. Mizuno, H. Murakami, I. Kawayama, Y. Takahashi, M. Yoshimura, Y. Mori, J. Darmo, and M. Tonouchi, "Scanning laser terahertz near-field imaging system," Opt. Express **20**(12), 12959–12965 (2012).
14. F. A. Hegmann, "Nanoscale imaging with terahertz scanning tunneling microscopy," Advanced Photonics 2016, SeTu3E.2 (2016).
15. K. Kawase, Y. Ogawa, Y. Watanabe, and H. Inoue, "Non-destructive terahertz imaging of illicit drugs using spectral fingerprints," Opt. Express **11**(20), 2549–2554 (2003).
16. M. H. Arbab, D. P. Winebrenner, T. C. Dickey, A. Chen, M. B. Klein, and P. D. Mourad, "Terahertz spectroscopy for the assessment of burn injuries in vivo," J. Biomed. Opt. **18**(7), 077004 (2013).

#303307 https://doi.org/10.1364/OE.25.022140
Journal © 2017 Received 26 Jul 2017; revised 29 Aug 2017; accepted 29 Aug 2017; published 1 Sep 2017

Optics EXPRESS

17. N. N. Zinov'ev, A. F. Fitzgerald, S. M. Strafford, D. J. Wood, F. A. Carmichael, R. E. Miles, M. A. Smith, and J. M. Chamberlain, "Identification of tooth decay using terahertz imaging and spectroscopy," Infrared and Millimeter Waves, 13–14 (2002).
18. B. M. Fischer, M. Walther, and P. U. Jepsen, "Far-infrared vibrational modes of DNA components studied by terahertz time-domain spectroscopy," Phys. Med. Biol. **47**(21), 3807–3814 (2002).
19. S. B. Kang, D. C. Chung, S.-J. Kim, J.-K. Chung, S.-Y. Park, K.-C. Kim, and M. H. Kwak, "Terahertz characterization of Y2O3-added AlN ceramics," Appl. Surf. Sci. **388**, 741–745 (2016).
20. T. Inagaki, I. D. Hartley, S. Tsuchikawa, and M. Reid, "Prediction of oven-dry density of wood by time-domain terahertz spectroscopy," Holzforschung **68**(1), 61–68 (2014).
21. S. Yu, B. J. Drouin, and J. C. Pearson, "Terahertz spectroscopy of the bending vibrations of acetylene 12C2H2," Astrophys. J. **705**(1), 786–790 (2009).
22. Y. C. Shen, T. Lo, P. F. Taday, B. E. Cole, W. R. Tribe, and M. C. Kemp, "Detection and identification of explosives using terahertz pulsed spectroscopic imaging," Appl. Phys. Lett. **86**(24), 241116 (2005).
23. N. Horiuchi, "Terahertz technology: Endless applications," Nat. Photonics **4**(3), 140 (2010).
24. N. T. Yardimci, H. Lu, and M. Jarrahi, "High power telecommunication-compatible photoconductive terahertz emitters based on plasmonic nano-antenna arrays," Appl. Phys. Lett. **109**(19), 191103 (2016).
25. A. A. Dubinov, A. Bylinkin, V. Y. Aleshkin, V. Ryzhii, T. Otsuji, and D. Svintsov, "Ultra-compact injection terahertz laser using the resonant inter-layer radiative transitions in multi-graphene-layer structure," Opt. Express **24**(26), 29603–29612 (2016).
26. T. Low and P. Avouris, "Graphene plasmonics for terahertz to mid-infrared applications," ACS Nano **8**(2), 1086–1101 (2014).
27. Y. Fan, N.-H. Shen, T. Koschny, and C. M. Soukoulis, "Tunable terahertz meta-surface with graphene cut-wires," ACS Photonics **2**(1), 151–156 (2015).
28. P. U. Jepsen, R. H. Jacobsen, and S. R. Keiding, "Generation and detection of terahertz pulses from biased semiconductor antennas," J. Opt. Soc. Am. B **13**(11), 2424–2436 (1996).
29. I. S. Gregory, C. Baker, W. R. Tribe, I. V. Bradley, M. J. Evans, E. H. Linfield, A. G. Davies, and M. Missous, "Optimization of photomixers and antennas for continuous-wave terahertz emission," IEEE J. Quantum Electron. **41**(5), 717–728 (2005).
30. E. R. Brown, F. W. Smith, and K. A. McIntosh, "Coherent millimeter-wave generation by heterodyne conversion in low-temperature-grown gaas photoconductors," J. Appl. Phys. **73**(3), 1480–1484 (1993).
31. C. W. Berry, M. R. Hashemi, S. Preu, H. Lu, A. C. Gossard, and M. Jarrahi, "High power terahertz generation using 1550 nm plasmonic photomixers," Appl. Phys. Lett. **105**(1), 011121 (2014).
32. F. Ospald, D. Maryenko, K. von Klitzing, D. C. Driscoll, M. P. Hanson, H. Lu, A. C. Gossard, and J. H. Smet, "1.55 μ m ultrafast photoconductive switches based on ErAs: InGaAs," Appl. Phys. Lett. **92**(13), 131117 (2008).
33. B. Sartorius, H. Roehle, H. Künzel, J. Böttcher, M. Schlak, D. Stanze, H. Venghaus, and M. Schell, "All-fiber terahertz time-domain spectrometer operating at 1.5 μm telecom wavelengths," Opt. Express **16**(13), 9565–9570 (2008).
34. A. Schwagmann, Z. Y. Zhao, F. Ospald, H. Lu, D. C. Driscoll, M. P. Hanson, A. C. Gossard, and J. H. Smet, "Terahertz emission characteristics of ErAs: InGaAs-based photoconductive antennas excited at 1.55 μm," Appl. Phys. Lett. **96**(14), 141108 (2010).
35. D. Stanze, A. Deninger, A. Roggenbuck, S. Schindler, M. Schlak, and B. Sartorius, "Compact cw terahertz spectrometer pumped at 1.5 μm wavelength," J. Infrared Millim. Terahertz Waves **32**(2), 225–232 (2011).
36. B. Globisch, R. J. B. Dietz, S. Nellen, T. Göbel, and M. Schell, "Terahertz detectors from Be-doped low-temperature grown InGaAs/InAlAs: Interplay of annealing and terahertz performance," AIP Adv. **6**(12), 125011 (2016).
37. B. Globisch, R. J. B. Dietz, D. Stanze, T. Göbel, and M. Schell, "Carrier dynamics in Beryllium doped low-temperature-grown InGaAs/InAlAs," Appl. Phys. Lett. **104**(17), 172103 (2014).
38. M. Mittendorff, M. Xu, R. J. Dietz, H. Kunzel, B. Sartorius, H. Schneider, M. Helm, and S. Winnerl, "Large area photoconductive terahertz emitter for 1.55 mum excitation based on an InGaAs heterostructure," Nanotechnology **24**(21), 214007 (2013).
39. I. Kostakis, D. Saeedkia, and M. Missous, "Terahertz generation and detection using low temperature grown InGaAs-InAlAs photoconductive antennas at 1.55," IEEE Trans. THz Sci. Technol. **2**(6), 617–622 (2012).
40. H. Roehle, R. J. Dietz, H. J. Hensel, J. Böttcher, H. Künzel, D. Stanze, M. Schell, and B. Sartorius, "Next generation 1.5 μm terahertz antennas: mesa-structuring of InGaAs/InAlAs photoconductive layers," Opt. Express **18**(3), 2296–2301 (2010).
41. M. Suzuki and M. Tonouchi, "Fe-implanted InGaAs terahertz emitters for 1.56μm wavelength excitation," Appl. Phys. Lett. **86**(5), 051104 (2005).
42. R. Takahashi, Y. Kawamura, T. Kagawa, and H. Iwamura, "Ultrafast 1.55-μm photoresponses in low-temperature-grown InGaAs/InAlAs quantum wells," Appl. Phys. Lett. **65**(14), 1790–1792 (1994).
43. C. Baker, I. S. Gregory, W. R. Tribe, I. V. Bradley, M. J. Evans, E. H. Linfield, and M. Missous, "Highly resistive annealed low-temperature-grown InGaAs with sub-500 fs carrier lifetimes," Appl. Phys. Lett. **85**(21), 4965–4967 (2004).
44. J.-M. Rämer, F. Ospald, G. von Freymann, and R. Beigang, "Generation and detection of terahertz radiation up to 4.5 THz by low-temperature grown GaAs photoconductive antennas excited at 1560 nm," Appl. Phys. Lett. **103**(2), 021119 (2013).

Optics EXPRESS

45. F. Fehsaraki, A. Jooshesh, V. Bahrami-Yekta, T. E. D. T. Tiedje, and R. Gordon, "Plasmonic anti-reflection coating for photoconductive terahertz generation," ACS Photonics **4**(6), 1350–1354 (2017).
46. A. Jooshesh, V. Bahrami-Yekta, J. Zhang, T. Tiedje, T. E. Darcie, and R. Gordon, "Plasmon-enhanced below bandgap photoconductive terahertz generation and detection," Nano Lett. **15**(12), 8306–8310 (2015).
47. L. L. Chang and A. Koma, "Interdiffusion between GaAs and AlAs," Appl. Phys. Lett. **29**(3), 138–141 (1976).
48. J. P. Leburton, K. Hess, N. Holonyak, Jr., J. J. Coleman, and M. Camras, "Index of refraction of AlAs-GaAs superlattices," J. Appl. Phys. **54**(7), 4230–4231 (1983).
49. D. E. Aspnes, J. P. Harbison, A. A. Studna, and L. T. Florez, "Application of reflectance difference spectroscopy to molecular-beam epitaxy growth of GaAs and AlAs," J. Vac. Sci. Technol. A **6**(3), 1327–1332 (1988).
50. M. Giehler, J. Herfort, W. Ulrici, L. Däweritz, and K. H. Ploog, "Optical properties of low-temperature grown GaAs on bragg reflectors," J. Appl. Phys. **92**(6), 2974–2976 (2002).
51. X. C. Zhang, X. F. Ma, Y. Jin, T. M. Lu, E. P. Boden, P. D. Phelps, K. R. Stewart, and C. P. Yakymyshyn, "Terahertz optical rectification from a nonlinear organic crystal," Appl. Phys. Lett. **61**(26), 3080–3082 (1992).
52. D. Gammon, B. V. Shanabrook, and D. S. Katzer, "Interfaces in GaAs/AlAs quantum well structures," Appl. Phys. Lett. **57**(25), 2710–2712 (1990).
53. D. E. Wohlert, K. L. Chang, H. C. Lin, K. C. Hsieh, and K. Y. Cheng, "Improvement of AlAs-GaAs interface roughness grown with high as overpressures," J. Vac. Sci. Technol. B **18**(3), 1590 (2000).
54. M. D. Sturge, "Optical absorption of gallium arsenide between 0.6 and 2.75 ev," Phys. Rev. **127**(3), 768–773 (1962).
55. S. U. Dankowski, D. Streb, M. Ruff, P. Kiesel, M. Kneissl, B. Knüpfer, G. H. Döhler, U. D. Keil, C. B. Sorenson, and A. K. Verma, "Above band gap absorption spectra of the arsenic antisite defect in low temperature grown GaAs and AlGaAs," Appl. Phys. Lett. **68**(1), 37–39 (1996).
56. K. M. Yu, M. Kaminska, and Z. Liliental-Weber, "Characterization of GaAs layers grown by low temperature molecular beam epitaxy using ion beam techniques," J. Appl. Phys. **72**(7), 2850–2856 (1992).
57. B. Heshmat, M. Masnadi-Shirazi, R. B. Lewis, J. Zhang, T. Tiedje, R. Gordon, and T. E. Darcie, "Enhanced Terahertz Bandwidth and Power from GaAsBi-based Sources," Adv. Opt. Mater. **1**(10), 714–719 (2013).
58. A. Jooshesh, L. Smith, M. Masnadi-Shirazi, V. Bahrami-Yekta, T. Tiedje, T. E. Darcie, and R. Gordon, "Nanoplasmonics enhanced terahertz sources," Opt. Express **22**(23), 27992–28001 (2014).
59. K. Sala, G. Kenney-Wallace, and G. Hall, "CW autocorrelation measurements of picosecond laser pulses," IEEE J. Quantum Electron. **16**(9), 990–996 (1980).
60. N. Vieweg, F. Rettich, A. Deninger, H. Roehle, R. Dietz, T. Göbel, and M. Schell, "Terahertz-time domain spectrometer with 90 dB peak dynamic range," J. Infrared Millim. Terahertz Waves **35**(10), 823–832 (2014).

1. Introduction

Terahertz (0.3 - 10 THz) systems have received a great deal of attention for applications in spectroscopy [1–8], imaging [5, 9–14], medicine [9, 15–18], material characterization [1, 9, 19–21], security [22, 23], and communication [24]. These applications require a compact, low cost and portable terahertz (THz) system to operate outside the laboratory environment, which is the goal of many recent works [25–27]. Among them, there is a growing interest in using photoconductive antennas (PCAs) as the most common approach for THz wave generation [28–30] and recent developments have been focused on PCAs operating in the telecom wavelength window [31–42] where low-cost high-power fiber-based components are available.

Whereas InGaAs is known as a common semiconductor material for telecommunication window absorption, it is more expensive, has lower conductivity and a longer carrier lifetime than low-temperature-grown GaAs (LT-GaAs) [36, 38, 43, 44]. In fact, plasmon-enhanced LT-GaAs (PE-LT-GaAs) operating at 1.57 µm can outperform InGaAs-based devices, as was previously demonstrated by our group [45, 46]. In this work, nearly an order of magnitude improvement in THz generation is achieved by adding an AlAs layer below the LT-GaAs and optimizing the As content and annealing conditions.

2. Experiment

Figure 1(a) shows a diagram of our time-domain THz setup, which was used to characterize PCAs as THz emitters. For alignment purposes only, we relied on second-harmonic generation in a periodically poled Lithium Niobate (PPLN) crystal that was used to drive a commercial LT-GaAs photoconductive switch (BATOP, PCA-40-05-10-800-a). All devices under test were pumped with 80 femtosecond pulse width at 1570 nm wavelength (PolarOnyx

Optics EXPRESS

- Mercury), which was ensured by implementation of double dichroic filters to eliminate the 785 nm fiber-laser pump wavelength.

Figure 1(b) is a drawing of a biased large-gap PCA under femtosecond laser pulse. We used a 30 µm long dipole antenna for all transmitters. Antennas were patterned on LT-GaAs using contact UV photolithography followed by sputter deposition of 5 nm titanium and 100 nm Gold. Conventional 5-µm-gap dipole PCAs were patterned and used for photoconductive material characterization and optimization. Additionally, closed-gap dipole antennas on the optimized material were patterned for plasmonic PCA fabrication to achieve maximum THz emission. Figure 1(c) is scanning electron microscopic (SEM) image of a slit PE-LT-GaAs PCA.

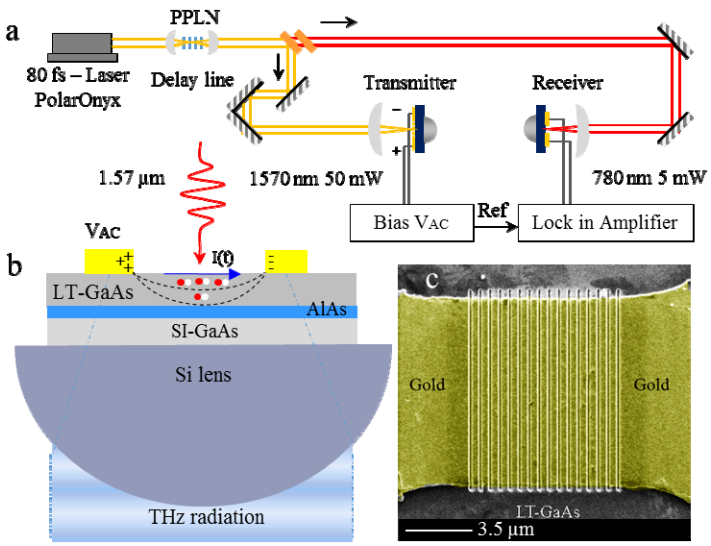

Fig. 1. (a) Free-space THz time-domain experimental setup. PPLN is Periodically Poled Lithium Niobate crystal and Bias V_{AC} is a square wave signal generator at 1kHz. (b) Schematic side view of a PCA with LT-GaAs/AlAs material. (c) SEM image of a PE-LT-GaAs with 490 nm periodicity slit plasmonic array.

3. Results and discussion

From a material growth perspective, THz emission of a LT-GaAs-based PCA operating below the semiconductor bandgap depends on three factors: annealing temperature, Gallium (Ga) to Arsenic (As) ratio, and thickness of the photoconductive material. Although more photocurrent is generated in a thick LT-GaAs material, lattice relaxation is a technical challenge in growing an extra thick LT-GaAs layer. Excessive As atoms cause tension and stress in the growing crystalline GaAs layer. With high As concentration, crystal relaxation starts at few hundred nanometers growth of the LT-GaAs layer. To find the optimum growth condition, we used simple 5 µm gap dipole antennas on various LT-GaAs substrates grown by molecular-beam epitaxy (MBE) at 226 °C to compare the onset of relaxation (i.e. maximum thickness) for each sample. Dark current, photocurrent and THz detected current of these PCAs were studied in our time-domain THz setup.

First, the effect of annealing was investigated. A 1 µm thick LT-GaAs layer was grown on SI-GaAs substrate. Thickness and As percentage of the annealed LT-GaAs layer was studied by X-ray diffraction (XRD) using a D8 Discovery Bruker XRD machine. Figure 2(a) plots XRD peaks separation of LT-GaAs (left peak) from SI-GaAs (right peak) for different annealing temperatures. Angular separation of the peaks is proportional to the As density of the LT-GaAs layer whereas the amplitude of the left peak indicates the thickness of the LT-GaAs. Comparing experimental results in Fig. 2(b) with XRD peaks separation from the

Optics EXPRESS

substrates in Fig. 2(a), we found that annealing at 550°C with 0.0078 degree angular peaks separation results in maximum THz signal amplitude and minimum dark current while maintaining As incorporation. Annealing at 600 °C and beyond is too high because the As clusters evaporate out. The decay in THz signal amplitude at high annealing temperatures is attributed to the reduction of mid-gap defects due to the escape of the excess As from the LT GaAs layer.

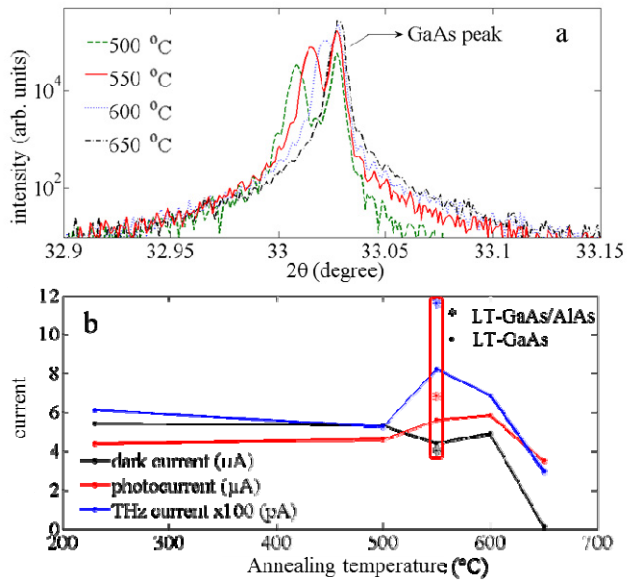

Fig. 2. (a) XRD peaks separation measurement for annealed LT-GaAs samples at different temperatures. (b) Photocurrent, dark current (with 5 V_{DC} bias), and THz current (with 20 V_{AC} bias) of simple dipoles fabricated on a 1 μm thick LT-GaAs substrate.

Next, we added an AlAs layer before the LT-GaAs layer while maintaining the optimized annealing conditions of the previous section. AlAs has a larger lattice constant than GaAs, which makes it possible to grow LT-GaAs with a larger lattice constant, allowing extra room for more excess As incorporation. Below bandgap light absorption in the LT-GaAs layer depends on mid-gap As defects. Thus, a rise in absorption is expected if As concentration is increased. It is noteworthy that XRD peaks separation greater than 0.025 degree was not achievable when LT-GaAs was grown directly on SI-GaAs substrate; however, when the AlAs layer was added, peaks separation as high as 0.031 degrees was achieved.

The higher AlAs bandgap energy of 2.16 eV has the additional advantages of preventing carrier diffusion into the SI-GaAs during laser exposure [47] and providing back reflection of transmitted light due to refractive index mismatch between AlAs and LT-GaAs [48–51]. We used 65 nm AlAs that is less than the quarter of the excitation wavelength (inside the material) required for optimal back-reflection; however, we have found that this is the maximum thickness that allows crystalline growth of LT-GaAs on AlAs [52, 53] in our MBE.

In an absorption experiment, a UDT S380 Optometer was used to measure the transmitted optical power through LT-GaAs samples with and without AlAs isolation layer. Figure 3 shows absorption and XRD angular peaks separation of the samples pumped by our 1570 nm femtosecond laser. Absorption was calculated from $1-P_s/P_r$, where P_s is the optical power measured from LT-GaAs based samples and P_r is the optical power measured from the same SI-GaAs substrate that was used to grow LT-GaAs layers (but without the LT-GaAs level). Absorption coefficient as high as 3000 cm^{-1} was obtained in our As-rich 600 nm thick LT-GaAs/AlAs sample, which has about one third of the absorption of GaAs near the intrinsic

Optics EXPRESS

bandgap edge [54]. In the literature, we have found absorption coefficients of up to 1200 cm^{-1}; which is much lower than the optimized structure achieved here [55].

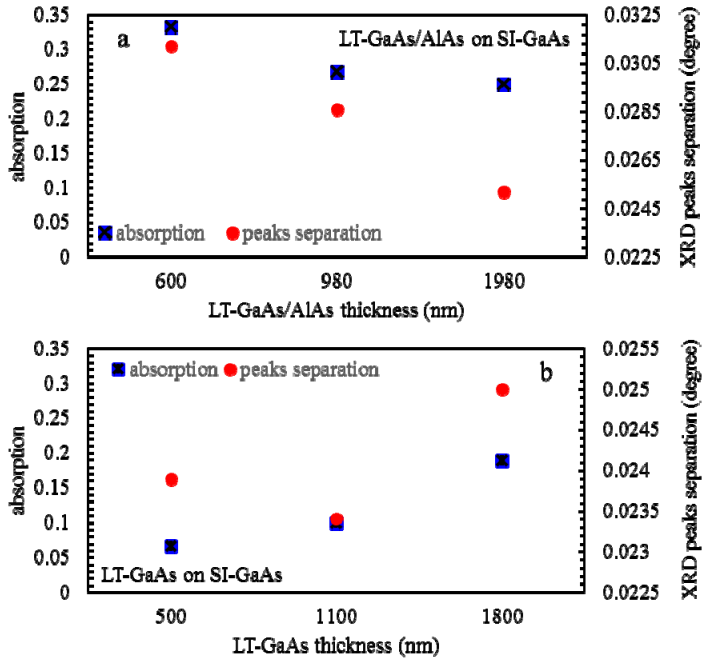

Fig. 3. Absorption percentage of as-grown LT-GaAs/AlAs and LT-GaAs substrates with high, medium and low As concentrations and respective thicknesses. Substrates were exposed to 1570 nm wavelength and transmitted power was normalized to the power recorded from a reference SI-GaAs.

Subsequently, 5-µm-gap dipole antennas were fabricated on 500 nm thick LT-GaAs/AlAs substrates with low, medium and high arsenic concentrations. XRD peaks separations of our low, medium and high arsenic concentration LT-GaAs are 0.0252, 0.0286 and 0.0312 degrees respectively. According to LT-GaAs layer characterization [56], we estimate excess As percentage of 0.5%, 0.58% and 0.66% for our low, medium and high LT-GaAs samples. Figure 4 compares THz current, dark current and photocurrents of the samples tested in our time-domain THz setup. Samples were biased at 20 V_{AC} and were illuminated with 50 mW of laser power at 1570 nm wavelength. While the As-rich LT-GaAs/AlAs PCA generated maximum photocurrent, this photocurrent did not transfer to a large THz signal amplitude. The fall in THz signal may be attributed to the rise in the dark current that reduces the on-off current ratio [57] and the mobility that is inversely proportional to the number of carriers. At 1.57 µm excitation, fewer carriers are generated in comparison with 0.8 µm excitation, which would increase the collision time and mobility of the material. In fact, a trade-off between the number of photo-generated carriers and mobility is required for efficient conversion of photocurrent to THz emission. In our measurements, the annealed PCA with medium excess As material has optimum THz emission at 1570 nm excitation. In addition, a medium excess As content LT-GaAs material has less dark current and noise, which is necessary in designing broadband THz receivers.

Optics EXPRESS

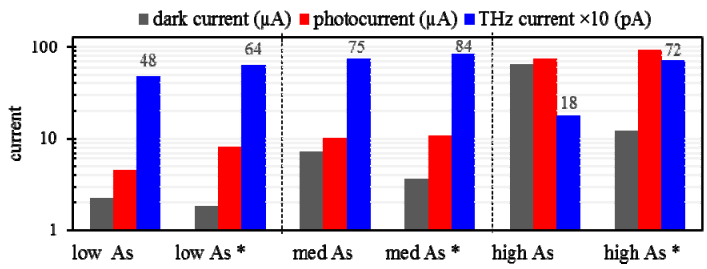

Fig. 4. THz received current (biased at 20 V_{DC}), photocurrent and dark current (biased at 5 V_{DC}) of PCAs with excess As of low (0.5%), med (0.58%) and high (0.66%) As concentrations. Samples with * were annealed at 550 °C for 1 minute.

Since we discovered that medium As actually gives the best response, we decided to use a thicker LT-GaAs layer to increase absorption. The thicker layer can tolerate the medium excess As concentration. Thus, we used a 2-μm-thick LT-GaAs/AlAs photoconductive material with medium excess As concentration for PE-LT-GaAs PCA fabrication. Periodicity and gap of the slit plasmonic array structure was optimized with the goal of minimizing the optical reflection coefficient (S_{11}) from the plasmonic structure using ANSYS HFSS software. A 490 nm periodicity with 100-nm-gap slit-array structure resulted in a minimized optical reflection according to the simulation. Johnson and Christy permittivity values and Palik permittivity values were used for modeling Gold and GaAs, respectively. The imaginary part of the GaAs permittivity at the telecom wavelength window was modified based on our experimental absorption results shown in Fig. 3.

An array of grooves was patterned through the Gold using focused ion beam (Hitachi FB-2100) to form periodic plasmonic structures. Through this process, Ga^+ ions imbed to a few nm depth of the LT-GaAs surface with the downside that these ions increase dark current and risk of failure at lower bias voltages. To avoid this problem, we placed samples in a diluted solution of HCL:H_2O (1:10) for 1 minute to remove Ga^+ ions from the surface. Using this recipe, resistance of the plasmonic gap area was increased to 1 MΩ, allowing a bias up to 100 V_{AC} without thermal breakdown.

We have previously shown that a tuned periodic plasmonic array maximizes the optical field coupling to the minimum depth of the substrate that results reflection as low as 8% [45]. Nano-structures also improve local electric field inside the photoconductive material where it is essential to accelerate carriers toward the conductors [46]. Plasmonic structures fill the gap area with gold that has more thermal conductivity than LT-GaAs. This will result in efficiently removing heat from the gap area allowing for operation at higher bias voltages and an extended thermal breakdown [58]. Nevertheless, the main contribution here is the effect of AlAs layer over and above the enhancement of the plasmonic structure.

Figure 5 shows our experimental results, demonstrating 15 times enhancement in THz emission from PE-LT-GaAs/AlAs sample in comparison with an InGaAs commercial emitter (BATOP, PCA-40-05-10-1550-a) at 1.57 μm wavelength at their maximum rated bias. The commercial BATOP transmitter is a single layer InGaAs based photoconductive antenna with anti-reflection coating that maximizes light coupling into the material. The (BATOP, PCA-40-05-10-1550-a) model has a 5 μm gap dipole antenna that allows maximum 3 V_{DC} bias according to its datasheet. The structure of this commercial PCA is the closest match to our devices.

The refractive index mismatch of the interface of GaAs (n_1 = 3.369) and AlAs (n_2 = 2.892) results in 22.7% back reflection into the LT-GaAs substrate and toward the reflective gold electrodes that would echo for few cycles. Comparing with a single pass scenario of the LT-GaAs on GaAs PCA, here light passes through a thicker absorptive material. The PE-LT-GaAs/AlAs PCAs with 17 nA peak to peak amplitude is about 7.2 nA higher than that of the

Optics EXPRESS

PE-LT-GaAs PCA. That makes the optical back reflection the dominant factor in improvement of signal amplitude even if a single cycle reflection from the interface and the gold electrodes is considered.

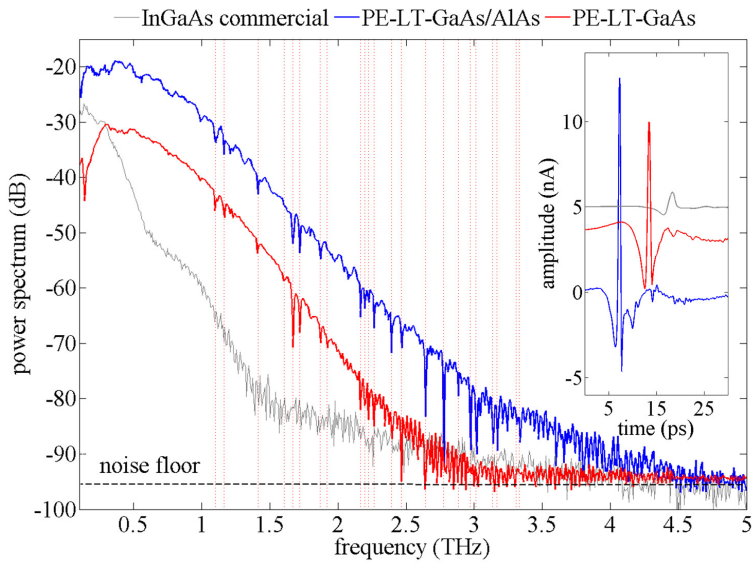

Fig. 5. THz spectrum response of the optimized PE-LT-GaAs/AlAs and InGaAs commercial samples. PE-LT-GaAs and PE-LT-GaAs/AlAs samples have an identical plasmonic structure whereas the commercial sample uses antireflection coating to maximize light coupling. Data obtained by averaging Fourier transforms for time domain THz pulses shown in the inset (40 scans – 90 seconds each with 30 ms integration time). Dashed lines are HITRAN water absorption lines.

Considering the similar carrier lifetime, sweep-out and noise for both the PE-LT-GaAs and PE-LT-GaAs/AlAs devices, only frequency components that have already overcame the noise floor in terms of spectral power will contribute to the bandwidth. Thus, the higher power PE-LT-GaAs/AlAs PCA has frequency components well above the noise floor resulting in an extended bandwidth up to 4.5 THz."

Here Fourier transform of 40 scans are averaged using MATLAB to obtain 75 dB dynamic range, which is 10 dB higher than a PCA without AlAs isolation layer. Each scan was 90 seconds long with 30 ms integration time. The 4.5 THz bandwidth is close to the theoretical limit ($\Delta f = 4.4\Delta\tau^{-1}$ where τ is the laser pulse width [59]) of our laser and it is comparable to the highest 5 THz bandwidth of the commercially available spectroscopy systems. Wider bandwidth and larger dynamic range is also achievable if more scans are being averaged. A 90 dB dynamic range has been reported by averaging 1000 scans of the THz signals generated and captured by the PCAs featuring 100 layers of InGaAs/InAlAs with a 60 femtosecond laser [60]. PE-LT-GaAs/AlAs photoconductive antennas deliver a comparable bandwidth in a few layer structure using a less expensive material system.

4. Conclusion

We have improved significantly the performance of a PE-LT-GaAs PCA by adding a thin AlAs isolation layer between the LT-GaAs and SI-GaAs layers. This isolated the charge carriers, provided optical back reflection and increased As incorporation to the level that is required to maximize terahertz generation. We note that the AlAs allows for even too-large As density, which deteriorates the material response by lowering the critical crystal growth thickness and increasing the dark current. A 2 μm thick LT-GaAs/AlAs with medium As density, annealed at 550°C for 1 minute resulted in the largest THz emission and bandwidth.

Optics EXPRESS

The optimized plasmon-enhanced LT-GaAs PCA operating below the bandgap that outperforms a commercial InGaAs PCA by factor of 15 with 4.5 THz bandwidth and 75 dB signal-to-noise ratio.

Funding

Natural Sciences and Engineering Research Council (NSERC) Canada Strategic Project Grant and Discovery Grant programs.

Acknowledgments

The authors declare that there are no competing financial interests.